The Astrophysical Journal, 683:178–188, 2008 August 10

STAR FORMATION IN THE MOST DISTANT MOLECULAR CLOUD IN THE EXTREME OUTER GALAXY: A LABORATORY OF STAR FORMATION IN AN EARLY EPOCH OF THE GALAXY'S FORMATION[1,2,3]

Naoto Kobayashi[4,5] and Chikako Yasui
Institute of Astronomy, School of Science, University of Tokyo, 2-21-1 Osawa, Mitaka, Tokyo 181-0015, Japan; naoto@ioa.s.u-tokyo.ac.jp

Alan T. Tokunaga[4]
Institute for Astronomy, University of Hawaii, 2680 Woodlawn Drive, Honolulu, HI 96822

and

Masao Saito
ALMA Project, National Astronomical Observatory of Japan, 2-21-1 Osawa, Mitaka, Tokyo 181-8588, Japan
Received 2007 August 3; accepted 2008 March 14

ABSTRACT

We report the discovery of active star formation in Digel's Cloud 2, which is one of the most distant giant molecular clouds known in the extreme outer Galaxy (EOG). At the probable Galactic radius of ∼20 kpc, Cloud 2 has a quite different environment from that in the solar neighborhood, including lower metallicity, much lower gas density, and small or no perturbation from the spiral arms. With new wide-field near-infrared (NIR) imaging that covers the entire Cloud 2, we discovered two young embedded star clusters located in the two dense cores of the cloud. Using our NIR and ^{12}CO data, as well as H I, radio continuum, and *IRAS* data in the archives, we discuss the detailed star formation processes in this unique environment. We show clear evidence of sequential star formation triggered by the nearby huge supernova remnant GSH 138-01-94. The two embedded clusters show a distinct morphology difference: the one in the northern molecular cloud core is a loose association with isolated-mode star formation, while the one in the southern molecular cloud core is a dense cluster with cluster-mode star formation. We propose that high compression due to the combination of the supernova remnant shell and an adjacent shell caused the dense cluster formation in the southern core. In view of the special environment, in particular the low-metallicity range, we suggest that the EOG could be an excellent laboratory for the study of star formation processes, such as those triggered by supernovae, that occurred during an early epoch of the Galaxy's formation. In particular, the study of the EOG may shed light on the origin and role of the thick disk, whose metallicity range well matches that of the EOG.

Subject headings: Galaxy: disk — Galaxy: formation — infrared: stars — ISM: clouds — open clusters and associations: general — stars: formation — stars: pre–main-sequence — supernova remnants

1. INTRODUCTION

The extreme outer Galaxy (EOG), which we define as the region with a Galactic radius (R_g) of more than 18 kpc, has a very different environment from the regions near our solar system, since it has a much lower gas density, lower metallicity (see the metallicity gradient curve in, e.g., Smartt & Rolleston 1997), and small or no perturbation from the spiral arms. Such a region is not only of strong interest in itself, but it also provides a good opportunity to study astronomical processes, such as star formation, in a physical environment that is very different from that of the solar neighborhood. While detailed star formation processes have been studied mostly for nearby star-forming regions at distances less than 1 kpc, where the physical/chemical environment appears to be relatively uniform, the EOG enables us to study how the environment (density, temperature, pressure, external radiation field, metallicity, etc.) affects the basic star formation processes and parameters such as the initial mass function, star formation efficiency, and disk formation efficiency.

Wouterloot & Brand (1989), Wouterloot et al. (1990), and Brand & Wouterloot (1995) obtained the first census of molecular clouds in the outer Galaxy based on the CO survey of *IRAS* point sources. Digel et al. (1994) found 11 molecular clouds, including Cloud 2, in the EOG based on CO observations of distant H I peaks in the Maryland-Green Bank survey (Westerhout & Wendlant 1982). Following those pioneering works, Heyer et al. (1998) conducted a comprehensive CO survey of molecular clouds in the outer Galaxy with the Five College Radio Astronomy Observatory (FCRAO) CO survey. Recently, Ruffle et al. (2007) conducted a molecular-line survey of some of the Digel clouds and provided maps and chemical modeling of Cloud 2. Such detailed study will eventually reveal how those molecular clouds were formed in the EOG. As for star formation activity, de Geus et al. (1993) first found an H II region associated with Digel's Cloud 2. Later, Kobayashi & Tokunaga (2000) found associated red infrared sources to confirm the star-forming activity in this cloud. Santos et al. (2000) and later Snell et al. (2002) found a considerable number of embedded star clusters in molecular clouds in the outer Galaxy that confirm that star formation in clusters is

[1] Based on data collected at the University of Hawaii 2.2 m telescope.
[2] This research has made use of the NASA/IPAC Infrared Science Archive, which is operated by the Jet Propulsion Laboratory, California Institute of Technology, under contract with the National Aeronautics and Space Administration.
[3] This research used the facilities of the Canadian Astronomy Data Centre, operated by the National Research Council of Canada with the support of the Canadian Space Agency.
[4] Visiting Astronomer, University of Hawaii 2.2 m telescope.
[5] Half of the work was done when visiting at the University of Hawaii during 1996–1999.

common in the outer Galaxy up to $R_g \sim 17$ kpc. Recently, Brand & Wouterloot (2007) also reported a discovery of an embedded cluster in a molecular cloud, WB 89-789, at the probable Galactic radius of ~20 kpc, which marks one of the most distant embedded clusters in the EOG.

Here we report the discovery of two embedded clusters in Digel's Cloud 2, which is one of the most distant molecular clouds in the EOG (Digel et al. 1994). While conducting a near-infrared (NIR) survey of the Digel clouds to study star formation activity in the EOG (Kobayashi & Tokunaga 2001), we found clear evidence of star formation activity in Cloud 2 (Kobayashi & Tokunaga 2000). As a follow-up study, we are extensively studying this cloud with deep NIR imaging using the Subaru 8.2 m telescope (Yasui et al. 2006, 2008) and with CO observations using the Nobeyama 45 m telescope (M. Saito et al. 2008, in preparation).

Originally, the kinematic distance to Cloud 2 was estimated at $R_g = 28$ kpc (heliocentric distance $D = 21$ kpc), while the latest H I observation by Stil & Irwin (2001) suggests $R_g = 23.6$ kpc ($D = 16.6$ kpc). Ruffle et al. (2007) use $R_g = 22$ and 28 kpc for their distance-sensitive calculations. However, several authors questioned this rather high R_g from independent distance estimates of the associated early-type star MR-1 (Muzzio & Rydgren 1974). The association of MR-1 with Cloud 2 appears to be quite firm based on the association of the Hα nebula (de Geus et al. 1993) and the photodissociation region (Kobayashi & Tokunaga 2000), and because all three components have almost the same LSR velocity: -102.4 km s^{-1} for Cloud 2 (Digel et al. 1994), -102.7 ± 12 km s^{-1} for MR-1 (Russeil et al. 2007), and -101 km s^{-1} for the Hα nebula (de Geus et al. 1993). Smartt et al. (1996) estimated the Galactic radius of MR-1 as $R_g = 15$–19 kpc ($D = 8$–12 kpc) with high-resolution optical spectra; the shorter and longer distances are based on LTE and non-LTE model stellar atmospheres. Recently, Russeil et al. (2007) reestimated the distance to MR-1 as $R_g = 14.3 \pm 0.5$ kpc ($D = 6.78 \pm 0.59$ kpc) using a newly obtained high-resolution optical spectrum and an LTE model stellar atmosphere, which is consistent with the LTE distance ($D = 8$ kpc) by Smartt et al. (1996). Because the spectroscopic distance of stars should be more accurate than the kinematic distance, the actual distance to Cloud 2 is likely to be that of MR-1, which is less than the kinematic distance calculated from H I/CO data. Throughout this paper, we adopt the most likely distance, $R_g = 19$ kpc ($D = 12$ kpc), for Cloud 2, the same one used in our previous paper (Kobayashi & Tokunaga 2000), because a non-LTE model is more likely to be accurate for stars in the effective temperature regime of MR-1 (Smartt et al. 1996). It is also the largest distance among those estimated by stellar spectroscopy and more consistent with the radio kinematic distances. When we discuss distance-sensitive parameters, we will mention the possible systematic uncertainty.

The ambient H I density at $R_g \sim 20$ kpc is thought to be very low because of the small surface density and the large scale height; $N_{\rm H\,I}$ could be as low as 0.001 cm^{-3} (e.g., Nakanishi & Sofue 2003). The metallicity of Cloud 2 is estimated at -0.7 dex from the radio molecular lines (Lubowich et al. 2004; see also Ruffle et al. 2005), which is consistent with the metallicity of MR-1 as measured by optical spectroscopy (-0.5 to -0.8 dex; Smartt et al. 1996; Rolleston et al. 2000).

The latest H I observation by Stil & Irwin (2001) revealed that a remarkably large supernova remnant (SNR) shell, GSH 138-01-94, is associated with Cloud 2. Because there is little or no perturbation from the spiral arms in the EOG environment, the supernova (SN) could have triggered star formation in Cloud 2. It is usually hard to determine what triggers star formation in the inner part of the Galactic disk because of the many chance projections of various foreground and background objects, and because the observed star-forming region itself has a complex structure of gas/dust and stars from its long star formation history and high ambient gas density. In such a region, a SNR shell cannot keep its uniform shape for a long enough time (e.g., a few Myr) to discern the SN-triggered star formation process because of the large amount of ambient material distributed nonuniformly. However, SNR shell expansion can be clearly observed in the EOG, which is free from the above complexity. Actually, GSH 138-01-94 shows a large complete SNR shell that has lasted for more than 4 Myr and is the largest and oldest SNR known in the Galaxy (Stil & Irwin 2001). Therefore, Cloud 2 is an excellent place to study SN-triggered star formation, which is thought to be one of the major star formation processes in galaxies (e.g., Elmegreen 2002).

The low metallicities in the EOG regions are comparable to those for Galactic thick-disk stars (e.g., Brewer & Carney 2006), dwarf irregular galaxies, and damped Lyα systems (e.g., Pettini 2004). In conjunction with the very low gas density and lack of spiral arm perturbation, the EOG may approximate the environment of star formation in the early universe. Because dwarf irregular galaxies have a similar environment—low metallicity, low gas density, and lack of spiral arm perturbation—they are also thought to represent the conditions of star formation in the early universe (e.g., Hunter et al. 2006). However, the EOG is advantageous for the study of such star formation processes simply because of its proximity compared to the galaxies in the local universe. Studies of the chemical composition of halo stars in our Galaxy show that star formation in the early epoch of the Galaxy's formation was mostly triggered by SNe (Ryan et al. 1996; Audouze & Silk 1995; Shigeyama & Tsujimoto 1998). Therefore, *Cloud 2 and other EOG star-forming regions are excellent laboratories in which to study the star formation process in an environment that is similar to that which existed during an early epoch of the Galaxy's formation*.

In this paper, we discuss our NIR and ^{12}CO observational results for Cloud 2 in the above context. We also make use of the mid-infrared (*IRAS*), H I, and radio continuum data in the archives for our discussion. The companion papers by Yasui et al. (2006, 2008) discuss very deep infrared imaging of the star-forming clusters with the Subaru 8.2 m telescope, and they reinforce our interpretation.

2. NEAR-INFRARED IMAGING

NIR images of Cloud 2 in the standard *J*-, *H*-, and *K*-band filters were obtained over a five night period (1998 October 3–7) using the QUick InfRared Camera (QUIRC) at the University of Hawaii 2.2 m telescope on Mauna Kea. QUIRC uses a 1024×1024 HgCdTe Astronomical Wide Area Infrared Imager (HAWAII) array and was used at the f/10 focus to provide a plate scale of $0.1886''$ pixel^{-1} with a field of view of roughly $3.2' \times 3.2'$. The entire arc-shaped Cloud 2 was covered with a mosaic of QUIRC fields. For this paper, we used only the data set of the third night, when the seeing conditions were best (~$0.5''$) and the star clusters were clearly resolved. The sky was covered with occasional thin cirrus on that night, but the photometric uncertainty due to the cirrus was insignificant. The total integration time was 5, 10, and 15 minutes for the *K*, *H*, and *J* bands, respectively.

All the data for each band were reduced with IRAF[6] with standard procedures: dark subtraction, flat-fielding, bad-pixel

[6] IRAF is distributed by the National Optical Astronomy Observatory, which is operated by the Association of Universities for Research in Astronomy, Inc., under cooperative agreement with the National Science Foundation.

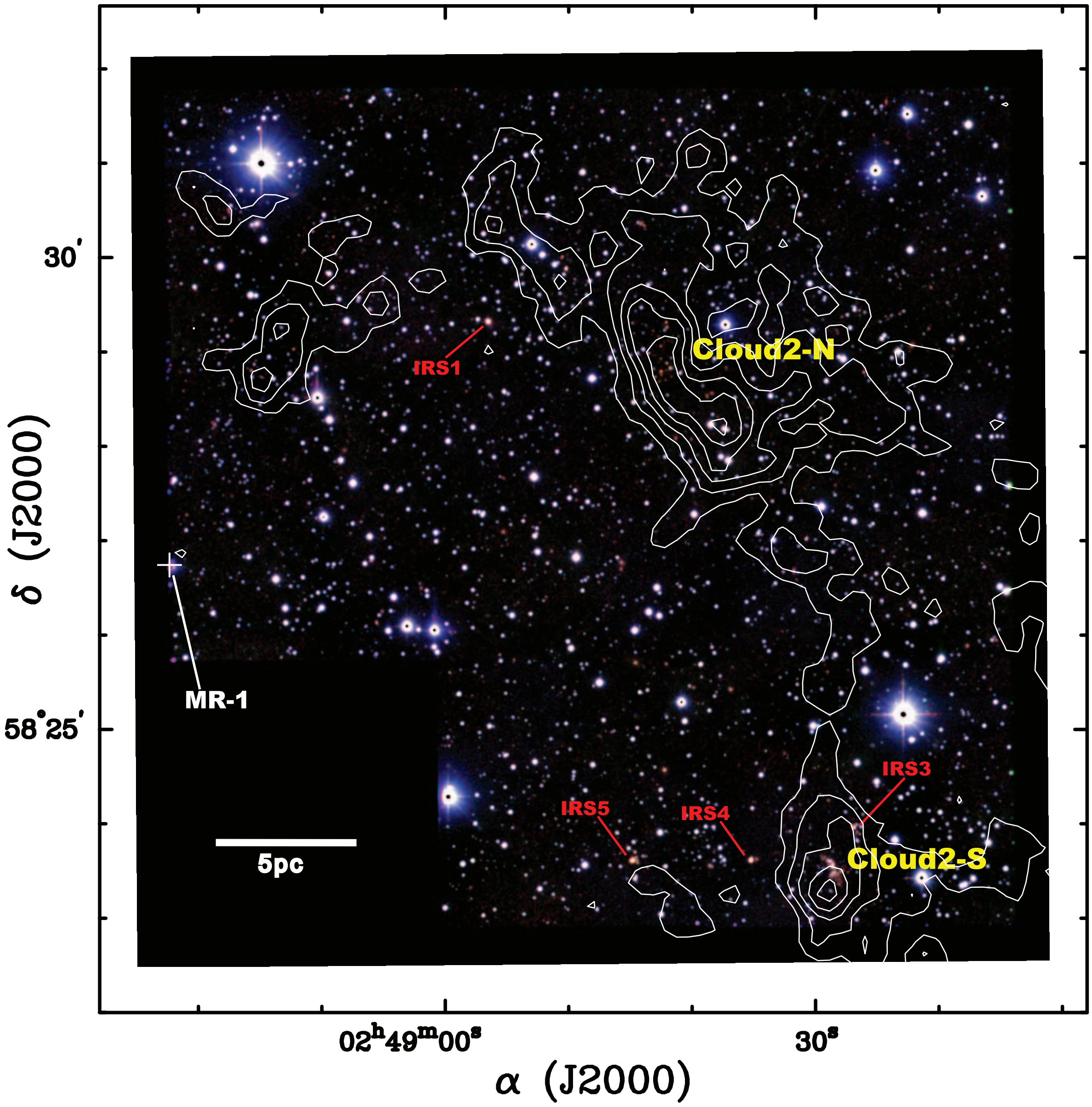

FIG. 1.—NIR *JHK* three-color image of Cloud 2 obtained with the QUIRC NIR camera. North is up, and east is to the left. The ^{12}CO (1–0) data obtained with the Nobeyama 45 m telescope are overplotted (*white contours*). The locations of bright NIR sources (IRS 1, 4, and 5; Kobayashi & Tokunaga 2000) and a visible early-type star, MR-1, are also indicated. A loosely packed embedded cluster (the Cloud 2-N cluster) is seen as an aggregation of red sources in the northern CO peak of the two CO peaks in Cloud 2-N. A dense embedded cluster (the Cloud 2-S cluster) is seen near the CO peak of Cloud 2-S. This cluster was originally identified as IRS 2 in Kobayashi & Tokunaga (2000). IRS 3, near Cloud 2-S, was also found to be a very small cluster (see also Fig. 2). Most other faint red sources in this field are faint background galaxies. The NIR image was Gaussian-convolved for viewing purposes. The resulting FWHM of the image is about 0.7″.

correction, median sky subtraction, image shifts with dithering offsets, and combining. The images of eight fields were combined into one large mosaic with standard IRAF image-matching tasks.

Figure 1 shows a *JHK* three-color image of Cloud 2 with ^{12}CO (1–0) contours overplotted (the radio data were newly obtained with the Nobeyama 45 m telescope). Locations of bright NIR sources identified by Kobayashi & Tokunaga (2000) and MR-1 (Muzzio & Rydgren 1974) are also indicated. In this infrared color image, two clusters of red sources (the Cloud 2-N and Cloud 2-S clusters) were identified in the two CO cores of the molecular cloud (Cloud 2-N and Cloud 2-S).[7] The Cloud 2-N cluster was first discovered with the QUIRC image, while the Cloud 2-S cluster was already recognized as an infrared source, IRS 2, in Kobayashi & Tokunaga (2000) and was resolved as a star cluster in the QUIRC image.

We performed photometry of those red sources and found that many of them have $H - K$ color excess in the $J - H$ versus $H - K$ color-color diagram. We presented the photometric properties of those red sources in companion papers by Yasui et al. (2006, 2008), in which we performed photometry with much higher photometric accuracy using deeper and higher resolution *JHK* images obtained with the Subaru 8.2 m telescope.

2.1. *Two Young Embedded Clusters*

Figure 2 shows the expanded images of both clusters. The Cloud 2-N cluster looks like a loose association similar to that in

[7] These two CO cores were originally called Cloud 2a and Cloud 2b, respectively, in Digel et al. (1994).

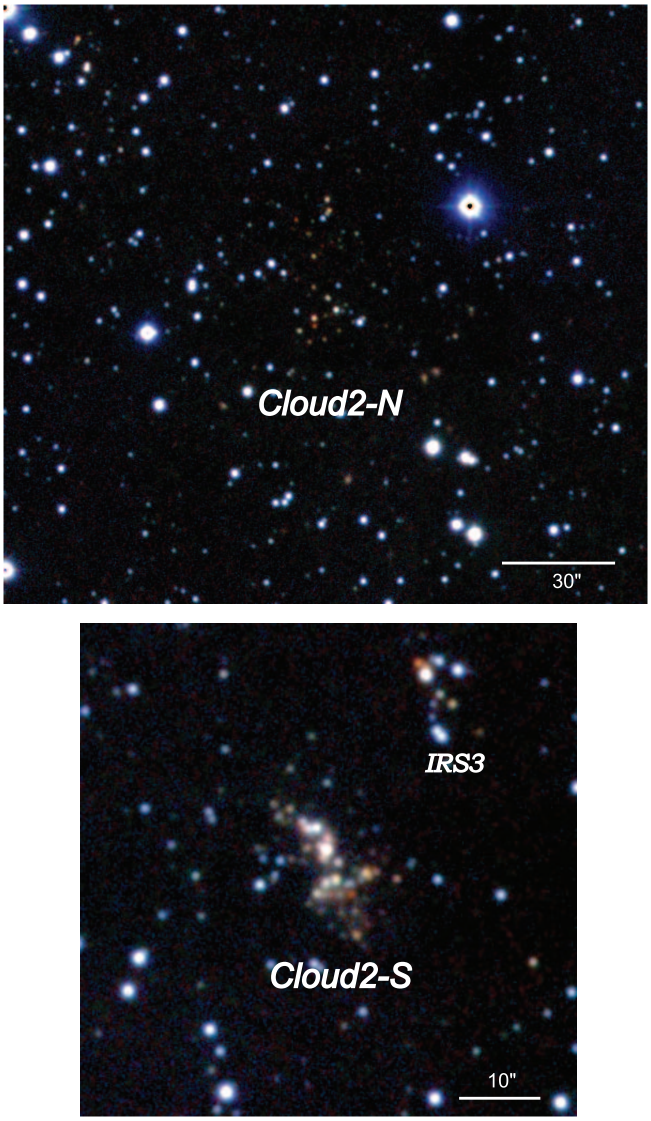

FIG. 2.—Expanded view of the *JHK* three-color image of the two embedded clusters (*top*, Cloud 2-N cluster; *bottom*, Cloud 2-S cluster). Note the difference in stellar density in those two clusters. IRS 3, near the Cloud 2-S cluster, is resolved into a very small cluster in this image.

the Taurus dark cloud (see, e.g., Lada et al. 1993), while the Cloud 2-S cluster shows more packed morphology, like that in the ρ Oph star-forming regions (see, e.g., Allen et al. 2007), suggesting the Cloud 2-N cluster is in *isolated star formation mode*, while the Cloud 2-S cluster is in *cluster star formation mode*. The Cloud 2-N and Cloud 2-S clusters are distributed over a region of ~1.5 and ~0.5 pc in diameter with stellar surface densities of about 10 and 50 stars pc^{-2}, respectively, assuming the heliocentric distance of 12 kpc. (See Yasui et al. 2008 for a more detailed analysis based on deeper images.) The density for Cloud 2-S is typical for young embedded clusters, but that of Cloud 2-N is less than the lower boundary for clusters listed in Lada & Lada (2003). There is a bright star at the center of the Cloud 2-S cluster. Assuming a distance modulus of 15.4, the *K*-band luminosity of the brightest star is $M_K \sim -0.4$, which is consistent with that of a late B-type star (Tokunaga 2000). Thus, the Cloud 2-S cluster seems to be a star cluster aggregating around a relatively massive star, most likely a Herbig Ae/Be star (see, e.g., Testi et al. 1999). If the heliocentric distance is 16.6 kpc as derived from the recent H I data (Stil & Irwin 2001), the above stellar densities are reduced by a factor of ~2, making the Cloud 2-N cluster a very loose association (~5 stars pc^{-2}), while the Cloud 2-S cluster is still a dense cluster with a typical density (~25 stars pc^{-2}). Also, the absolute magnitude of the brightest star of the Cloud 2-S cluster becomes $M_K \sim -1.1$, which is consistent with that of an early-to-mid B-type star (Tokunaga 2000). Therefore, the above conclusion regarding isolated and cluster star formation modes still holds despite the possible distance uncertainty.

2.2. *Isolated Bright Young Stellar Objects*

Kobayashi & Tokunaga (2000) found several bright young stellar objects (YSOs) in and around Cloud 2. Besides IRS 2 and 3, which are resolved as clusters in Cloud 2-S, other IRS sources (IRS 1, 4, and 5) are also detected and resolved in our new images (Fig. 3). Those bright isolated infrared stars are located eastward of the molecular cloud (see Fig. 1). Their *K*-band absolute magnitudes ($M_K = -2.4, -1.3$, and -2.2; Kobayashi & Tokunaga 2000) and $H - K$ excess suggest all of them are dust-enshrouded intermediate-mass stars, probably Herbig Ae/Be stars. IRS 1, which is just outside Cloud 2-N, appears to be a single star, but it has an extended nebulosity in the northeast-southwest direction (see Fig. 3, *left*), suggesting it is a YSO with outflow activity. IRS 4 and 5, which are eastward of Cloud 2-S, have faint red

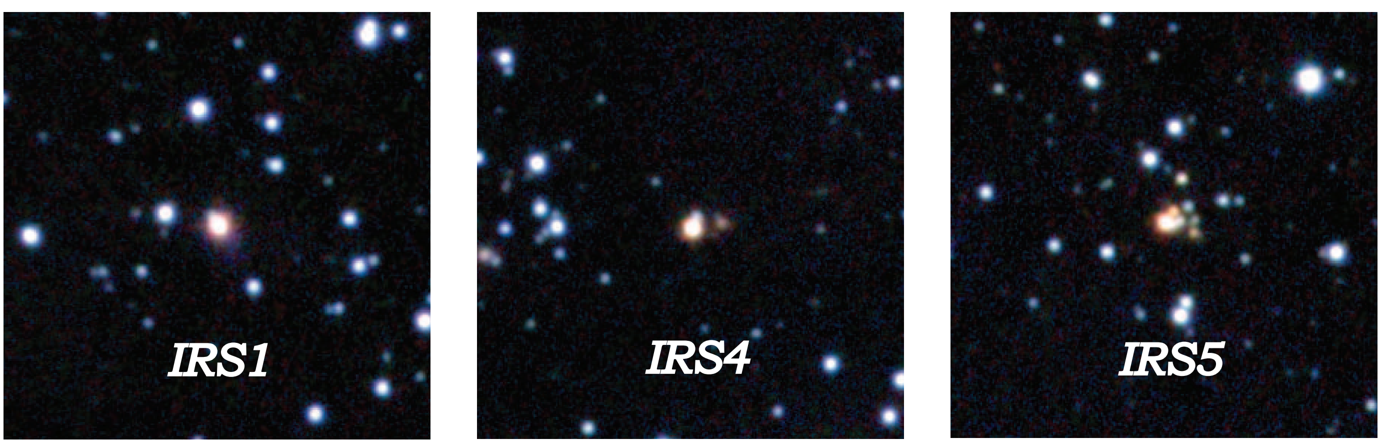

FIG. 3.—Expanded view of the *JHK* three-color image of the bright NIR sources near Cloud 2. Each box shows 30″ square. North is up, and east is to the left. These sources are identified as intermediate-mass YSOs (Herbig Ae/Be stars). IRS 1 shows a faint nebulosity extended to the southwest, which would be an outflow or a reflection nebula. IRS 4 and 5 show several faint red companion stars to the west, forming very small clusters.

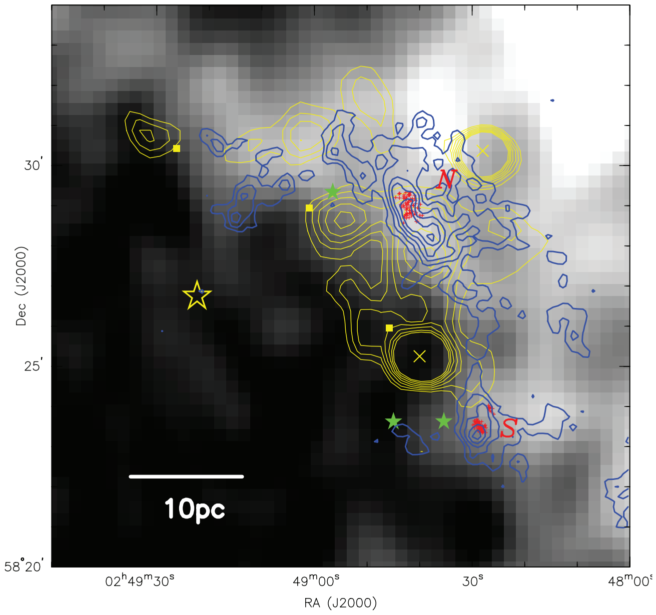

Fig. 4.—Summary of star formation activities in Cloud 2. A gray-scale image and blue contours show the distribution of H i and ^{12}CO (1–0) emission integrated over the velocity range −94 to −105 km s^{-1}. Yellow contours show the 1.4 GHz radio continuum from NVSS data; note that the two brightest pointlike sources (*crosses*) are unrelated foreground/background radio sources. Filled yellow squares show the peaks of Hα nebulae (de Geus et al. 1993). The open yellow star and filled green stars show MR-1 and bright NIR sources, respectively. The locations of the members in the Cloud 2-N and Cloud 2-S clusters and the Cloud 2-S minicluster are shown with red plus signs. Although the spatial resolution of the H i image and the VLA map is originally 1′ and 45″, respectively, here they are Gaussian-convolved with 1 pixel (18″ and 15″, respectively) for better viewing. The beam size of the Nobeyama CO map is about 20″. See the discussion in the text for details.

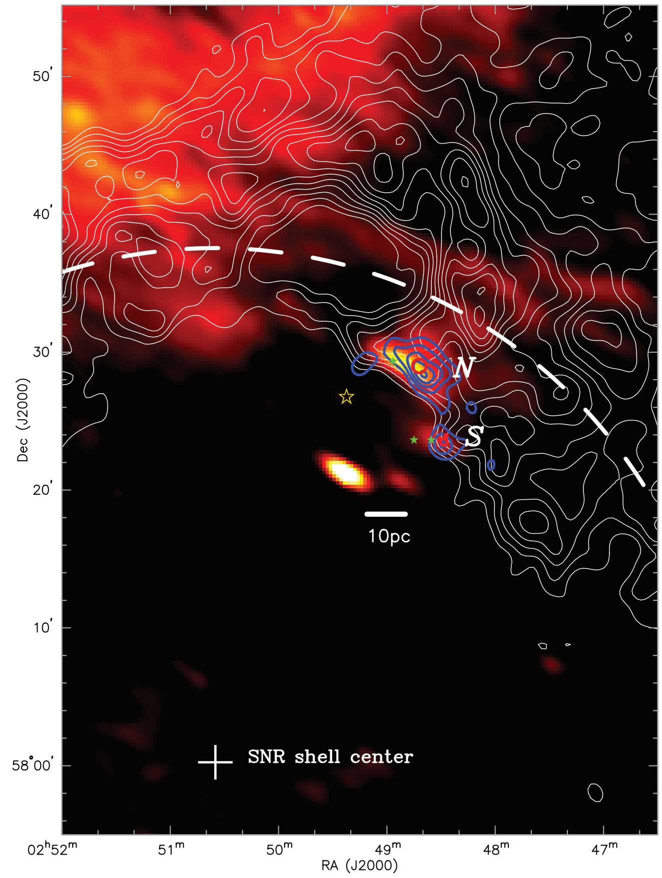

Fig. 5.—Locations of Cloud 2 and forming stars with respect to the SNR shell GSH 138-01-94 (Stil & Irwin 2001). The center of the shell is shown with a white plus sign, while the edge of the shell is shown with a dashed line. White contours show the H i surface brightness integrated over the velocity range v_{LSR} = −94 to −105 km s^{-1} (from CGPS data), while the blue contours show the ^{12}CO (1–0) surface brightness (from our Nobeyama data). The background image is the *IRAS* 60 μm image from *IRAS* IGA data. The open yellow star, filled green stars, and red circles show the locations of the visible early-type star MR-1, the bright NIR sources, and the two embedded clusters, respectively. The H i and *IRAS* images are 1 and 2 pixel Gaussian-convolved, respectively, for better comparison to the CO map. The bright *IRAS* source in the center of the image is an unrelated foreground object (a combination of two bright NIR sources, IRS 6 and 7 in Kobayashi & Tokunaga 2000) and shows the average PSF of this *IRAS* image. See the discussion in the text for details.

companion stars to the west (see Fig. 3, *middle and right*), suggesting they form typical small aggregations around intermediate-mass stars (Testi et al. 1999).

In our NIR images, IRS 1, 4, and 5, as well as MR-1, do not show a cluster with a considerable number (e.g., >10) of NIR sources at parsec scales, as do the two embedded clusters. They appear to be isolated bright objects. Kobayashi & Tokunaga (2000) argued that those bright YSOs are associated with Cloud 2 because of their proximity to the cloud and also because bright red sources were found only near Cloud 2 in their entire surveyed area of $34' \times 40'$. Also, one of the sources, IRS 5, accompanies a small molecular cloud core extending from the Cloud 2-S core toward the southwest (Fig. 1). Therefore, their association with Cloud 2 appears to be quite firm.

3. STAR FORMATION IN CLOUD 2

3.1. *Overall Activity and Geometry*

Besides the clusters and the isolated YSOs, other star formation–related activities are known in the Cloud 2 region. Soon after the discovery of Cloud 2, de Geus et al. (1993) discovered an associated extended H ii region with an Hα emission line, and a visible early-type star, MR-1, which had already been found by an independent blue star search in the outer Galaxy (Muzzio & Rydgren 1974), was recognized as a probable exciting source of the H ii region. Stil & Irwin (2001) found extended 21 cm (1.4 GHz) continuum emission projected on Cloud 2-N and located on the maxima of the Hα intensity map of de Geus et al. (1993). Based on the correlation with Hα and the absence of a counterpart at 74 cm, Stil & Irwin (2001) suggested that the continuum emission is thermal emission from an H ii region.

Figure 4 summarizes the star formation activities in Cloud 2: the locations of NIR objects and MR-1 are overplotted on the H i 21 cm gray-scale image,[8] 1.4 GHz radio continuum contour,[9] and ^{12}CO (1–0) contour from our Nobeyama data. Figure 4 clearly shows that the CO emission delineates the inner edge of the SNR H i shell, whose center is located toward the bottom left side of this image. Stil & Irwin (2001) first suggested that Cloud 2 is associated with the approaching (blueshifted) side of the H i shell based on the coincidence of the sky position and the line-of-sight velocities (v_{LSR} = −103.6 km s^{-1} for ^{12}CO and −101.9 km s^{-1} for H i). The CO cloud is located by the approaching side of the H i shell, as if it delineates the inner side of the shell (Fig. 4; see also Fig. 5). Because the radial velocities

[8] From Canadian Galactic Plane Survey (CGPS) data at http://www1.cadc-ccda.hia-iha.nrc-cnrc.gc.ca/cgps/.

[9] From NRAO/VLA Sky Survey (NVSS) data at http://www.cv.nrao.edu/nvss/ (Condon et al. 1998).

of CO and H I clouds are consistent with that for the H II region ($v_{LSR} = -101$ km s^{-1} from Fabry-Pérot Hα imaging; de Geus et al. 1993), it is highly likely that H I, CO, and the H II region are associated with each other at the same distance from us. The radial velocity of the visible early-type star MR-1 was measured at $v_{LSR} = -102.7 \pm 12$ km s^{-1} by Russeil et al. (2007), and this high velocity is also quite consistent with the velocities of the warm and cold gas components. Some runaway OB stars with this velocity have been observed in the I Per OB association (McLachlan & Nandy 1985), which is associated with the foreground Perseus arm but relatively close to Cloud 2 on the sky with an angular distance of about 3°–5°. However, because most of the OB stars in the association have $v_{LSR} = -30$ to -50 km s^{-1}, which is the typical velocity for the Perseus arm, it would be quite safe to say that MR-1, with a much higher velocity, is associated with Cloud 2, which is located far beyond the Perseus arm. We can therefore conclude that all those objects in Figure 4 (from the H I cloud to the NIR clusters) are associated with each other at the same distance.

De Geus et al. (1993) found that the three intensity maxima of Hα (in their Fig. 3), which are shown in Figure 4 (*squares*), match well with the extended features of the 1.4 GHz continuum, which strongly supports the suggestion by Stil & Irwin (2001) that the radio continuum is coincident with the H II region in this star-forming region. The radio continuum emission extends from near the CO cloud to the east toward MR-1 (*open yellow star*). This suggests that the H II region is excited mainly by MR-1 but partly by the IRS sources (*filled green stars*). We have also noticed that one more strong radio continuum peak is located just 1′–2′ south of the Cloud 2-N cluster (Fig. 4). This strong peak is not seen in the Hα images by de Geus et al. (1993); rather, their image shows a local minimum of the Hα emission near this radio continuum peak. Therefore, the H II gas of this extended radio continuum feature may be located *behind* the CO cloud, which should hide the accompanying Hα emission by strong dust extinction. This view is consistent with the fact that all the stars in the Cloud 2-N cluster are behind the CO cloud with a uniform extinction of $A_V \sim 4$ mag, as found by Yasui et al. (2008);[10] we are seeing the Cloud 2-N cluster and the H II emission feature through the moderately thick molecular cloud. Unlike Cloud 2-N, Cloud 2-S does not seem to be under the strong influence of photoionization by MR-1 and/or the bright NIR sources.

Figure 5 shows Cloud 2 and the cloud members on the *IRAS* 60 μm image,[11] as well as the H I emission contour of the SNR shell. An extended *IRAS* source, IRAS 02450+5816, which is bright at 60 and 100 μm, is located between MR-1 and Cloud 2-N and is identified as a photodissociation region formed by MR-1 and/or IRS 1 (Kobayashi & Tokunaga 2000). The Cloud 2-S cluster is in the vicinity of an unresolved *IRAS* source, IRAS 02447+5811, which is bright only at 60 μm (see Table 2 in Kobayashi & Tokunaga 2000) and is most likely related to the relatively hotter dust around the bright YSO in the center of the Cloud 2-S cluster. There might be some contribution to the *IRAS* flux of IRAS 02447+5811 from other bright isolated YSOs, IRS 4 and 5, because its *IRAS* 60 μm image appears to extend slightly toward those bright isolated YSOs (Fig. 5). We have checked mid-infrared images by the *Midcourse Space Experiment* (*MSX*)[12] at 8–21 μm but could not find any clear counterpart to the Cloud 2-N and 2-S clusters, as well as the bright isolated YSOs. Although the very extended 60 μm features at the top of Figure 5 are accompanied mostly by unrelated foreground clouds and star-forming regions, some of the features (like the filamentary feature just outside the H I shell delineated by the dashed white line) might be related to the H I shell.

3.2. *Sequential Star Formation*

The CO cloud has an arc shape (Figs. 1, 4, and 5) that is well aligned with the H I SNR shell GSH 138-01-94 and open toward the center of the shell (Fig. 5), showing that the CO cloud is clearly affected by the SNR H I shell. The clusters are associated with the two densest CO peaks of Cloud 2, and the sharp CO contours from the cluster toward the center of the SNR shell (Fig. 1; see also the CO 2–1 map in Ruffle et al. 2007) suggest that the compression of molecular gas triggered star formation. In Cloud 2-N, the cluster is associated with the northeastern subpeak, which appears to be more strongly compressed in the expansion direction than the southwestern subpeak, which does not harbor any clear star formation activity.

The young stars in and around Cloud 2 appear to show an age sequence from east to west following the direction of the SNR shell expansion. Compared to the visible early-type star MR-1, the bright NIR sources IRS 1, 4, and 5 apparently form a younger stellar population with redder colors and locations closer to the molecular cloud. Although IRS 5 may have a small molecular cloud core extending toward the southwest (see Figs. 1 and 4), all three sources are not directly associated with the massive molecular clouds, as are the two embedded clusters. While the clusters are visible only in the NIR, we confirmed that IRS 1, 4, and 5 are marginally visible in the DSS2 *R*-band and IR-band plates. These facts suggest that the bright NIR sources are less embedded and older than the embedded clusters. In summary, there is an age sequence (old to young) from the visible early-type star, MR-1, to the isolated intermediate-mass infrared stars IRS 1, 4, and 5, and finally to the two embedded clusters in the molecular clouds. The direction of the age sequence following that of the SNR shell expansion (see Fig. 4) suggests *sequential star formation* triggered by the SN explosion.

Was the formation of MR-1 triggered by the SNR shell, or was it coincidentally situated there before the SN explosion? The age of the SNR shell was originally estimated at 4.3 Myr by Stil & Irwin (2001). Because the expansion age is in proportion to the shell radius in Stil & Irwin's model,[13] it can be as low as 3.0 Myr for our assumed distance ($D = 12$ kpc) or as much as 4.3 Myr for the Stil & Irwin assumed distance ($D = 16.6$ kpc). On the other hand, it is difficult to estimate the age of MR-1. Its spectral type was estimated at B0–B1 (Muzzio & Rydgren 1974; Smartt et al. 1996), suggesting that its mass is about 20 $M_\odot$ and its age is no more than 10 Myr if it is on the main sequence. Smartt et al. (1996) suggested that judging from its low gravity, $\log g = 3.7 \pm 0.1$, MR-1 is likely just evolving off the main sequence, while that of a B0–B1 V star is $\log g = 3.9$ (Drilling & Landolt 2000). In this case, the age of MR-1 should be greater than 10 Myr, and the star should have been located there before the SN explosion. However, Russeil et al. (2007) recently reestimated the spectral type of MR-1 as O9 V (thus, a higher effective temperature with an ~2000 K increase) with newly obtained high-resolution spectra.

[10] They originally suggested a total extinction of $A_V \sim 7$ mag toward the Cloud 2-N cluster in Yasui et al. (2006), but the value became slightly smaller ($A_V \sim 6$) after reanalyzing the data (Yasui et al. 2008). The contribution from Cloud 2 only is $A_V \sim 4$ mag after subtracting the contribution from the foreground ISM ($A_V \sim 2$ mag). This extinction is consistent with Ruffle et al. (2007), who suggested $A_V < 4$ mag based on their submillimeter observations and a lower than average dust-to-gas ratio in the low-metallicity cloud.

[11] From the *IRAS* Galaxy Atlas at IPAC, http://irsa.ipac.caltech.edu/data/IGA/.

[12] From the *MSX* Data Atlas at IPAC, http://irsa.ipac.caltech.edu/data/MSX/.

[13] In their model the expansion radius R is in proportion to $t^{2/7}$.

This suggests that MR-1 could well be still on the main sequence. Because Smartt et al.'s suggestion was based on a 0.2 dex difference in gravity (with the uncertainty of 0.1 dex), and because there is an effective temperature uncertainty as shown by Russeil et al.'s new observation, it would be hard to conclude that MR-1 is just evolving off the main sequence. In this case, the age of MR-1 could be much less than 10 Myr. Because there is no convincing method to measure the age of a star on the main sequence, it would be difficult to precisely determine the age of MR-1 with the accuracy necessary to compare its age with that of the SNR shell. Although there is a small possibility that MR-1 formed in situ prior to the SN explosion, we suggest that the formation of MR-1 was triggered by the SNR shell in view of the small probability that the sequence of YSOs observed is by chance. In this scenario, the age of MR-1 can be as much as the age of the SNR shell (3 Myr) and most likely about 2 Myr in view of the location of MR-1 with respect to the current SNR shell (see discussion in § 4.2 for the age estimate with the SN trigger model). In § 4 we discuss the process of SN-triggered star formation in Cloud 2 in more detail, assuming that MR-1 is the first object formed by the SNR shell.

4. SUPERNOVA-TRIGGERED STAR FORMATION

4.1. *Cloud Formation*

Stil & Irwin (2001) concluded that the expanding H I shell, GSH 138-01-94, was formed by a SN because of the nonexistence of any OB association inside the shell. Although there is no conclusive evidence for the SN explosion itself, as there is for the nearby SNR H I shells with radio continuum and X-ray emission, this interpretation appears to be quite solid in view of the observed properties, e.g., the perfectly spherical shell with a very large diameter that can survive only in a very low gas density environment with little or no perturbation from other objects.

Stil & Irwin (2001) suggested that Cloud 2 is associated with the approaching (blueshifted) side of the H I shell based on the coincidence of the sky position (see Fig. 5) and the line-of-sight velocities ($v_{\rm LSR} = -103.6$ km s^{-1} for ^{12}CO and -101.9 km s^{-1} for H I, while the center velocity of the expanding shell is $v_{\rm LSR} = -94.2$ km s^{-1}). Recently, Ruffle et al. (2007) concluded that the SNR H I shell has interacted with Cloud 2 based on extensively observed and modeled molecular chemistry for Cloud 2. They suggest that the chemistry of Cloud 2 is a direct result of shock fronts from the SNR H I shell propagating through the cloud sometime between 10^3 and 10^4 yr ago (see also Ruffle 2006). At the EOG, there is also no confusion with other objects because there is no complex star formation history and there is very low gas density and little perturbation from the spiral arms. Therefore, we can conclude that the H I shell and the molecular cloud are closely associated.

The shape of the molecular cloud follows the H I shell (Figs. 4 and 5), and this suggests that the formation of the molecular cloud itself was related to the SNR shell. Ruffle et al. (2007) considered the possibility that the cloud was formed by the H I shell from swept-up interstellar gas through Rayleigh-Taylor instabilities. However, it is expected that the formation of a molecular cloud is slowed down in the low-metallicity environment because the formation of H_2 molecules requires dust particles (e.g., see § 4.6 in Dyson & Williams 1997), and there is less dust in the low-metallicity environment. Typically, it takes 30 Myr to form a giant molecular cloud, even under conditions of solar metallicity (e.g., Tielens 2005), and it could take even longer in Cloud 2 in view of its very low dust content (Ruffle et al. 2007). This formation timescale is much longer than the age of the SNR shell (~3 Myr). Therefore, it is likely that the molecular cloud was already there before the SN explosion and that the SN shock that passed through the molecular cloud formed the shape of the cloud (P. Ruffle 2008, private communication), although we cannot completely exclude the possibility that the molecular cloud was formed by the SN shock. The cloud formation process itself in such low-metallicity environments still remains an important open question.

4.2. *Star Formation*

The steep CO contour on the inner side of the SNR shell for both Cloud 2-N and Cloud 2-S (Figs. 1 and 4) strongly suggests that the compression of the molecular cloud was brought on by the H I shell expansion. Some portion of the compression could be produced by the stellar wind from the formation of the first star, MR-1, as a secondary process of the SN explosion. The H II region (Fig. 4), which extends in and around Cloud 2-N, clearly shows that at least Cloud 2-N is strongly affected by MR-1. However, Cloud 2-S does not have either an associated Hα/radio continuum (Fig. 4) or a photodissociation region (Fig. 5), which suggests that Cloud 2-S was compressed purely by the SNR shell.

If the passage of the SNR shell has triggered cluster formation in Cloud 2, the upper limit of the age of the cluster can be estimated from the projected angular difference of the cluster from the current SNR shell front. Figure 6 shows that the projected angular difference is about 300″. Because the projected angular radius of the H I SNR shell is 2238″ and its age estimated for our assumed distance, $D = 12$ kpc (see discussion in § 3.2), is 3.0 Myr, the projected angular difference suggests that the cluster is younger than $300/2238 \times 3.0 \sim 0.4$ Myr. Although the shell expansion speed is expected to decline with time, that only shortens the upper limit. Therefore, the age upper limit of 0.4 Myr still holds. It is very interesting to note that this age estimate is in quite good agreement with an independent age estimate of the Cloud 2-N cluster by Yasui et al. (2006), who estimated the age of the cluster at about 0.5 Myr from modeling of the *K*-band luminosity function. This consistency strongly supports the idea that the cluster formation was basically triggered by the SNR. Note that the SN shell would have moved more slowly through the denser material of Cloud 2 because of mass conservation. This possible slow expansion may cause some systematic uncertainty of the above age estimate.

4.3. *Isolated- and Cluster-Mode Star Formation*

The two embedded clusters show a distinct morphology difference: the one in the northern molecular cloud core is a loose association with an isolated star formation mode, while the one in the southern molecular cloud core is a dense cluster with a cluster star formation mode. Because the cloud mass of both Cloud 2-N and Cloud 2-S are similar ($\sim 5 \times 10^3\ M_\odot$;[14] Digel et al. 1994; Ruffle et al. 2007), the difference in the appearance of the two clusters may give us a good opportunity to study what causes the differences between the two star formation modes.

[14] Originally, Digel et al. (1994) estimated the cloud mass to be $\sim 10^4\ M_\odot$, assuming a kinematic distance of $D = 21$ kpc ($R_g = 28$ kpc). The present number was converted from the original estimate assuming a distance of $D = 12$ kpc ($R_g = 19$ kpc). Ruffle et al. (2007) also calculate the cloud mass of both Cloud 2-N and Cloud 2-S as $\sim 5 \times 10^3\ M_\odot$ for the distance of 14–20 kpc ($R_g = 22$–28 kpc) using observed column densities and large velocity gradient models.

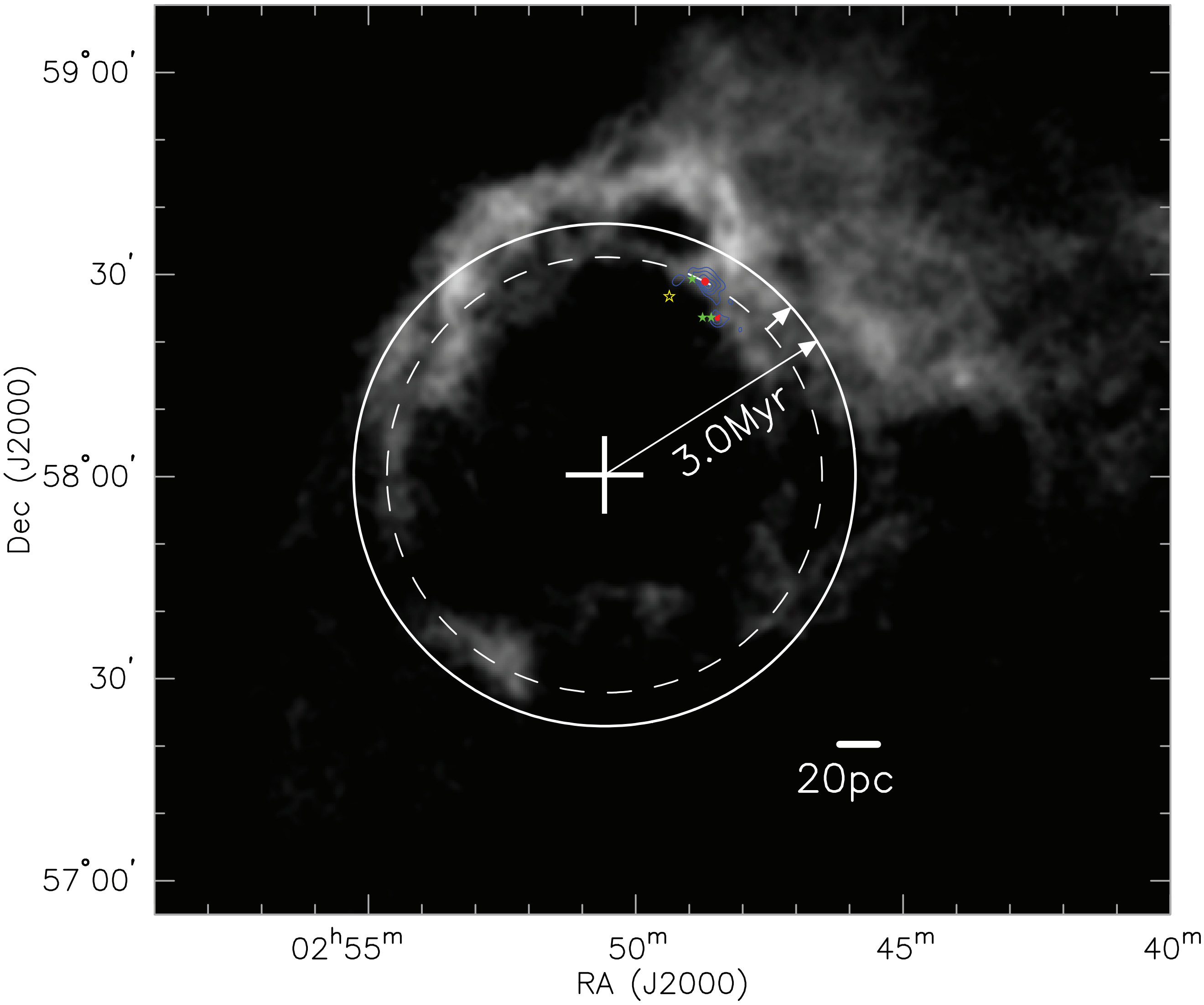

FIG. 6.—Location of Cloud 2 and the star clusters in the SNR shell GSH 138-01-94. The gray-scale image and blue contours show the H I and CO in $v_{\rm LSR} = -94$ to -105 km s^{-1}. The filled red circles show the location of the young embedded clusters. The solid circle shows the current location of the SNR shell with an estimated age of 3.0 Myr (see § 4.2). The dashed circle shows the location of the Cloud 2-N cluster. The small arrow shows the projected separation of 300″, from which the lifetime of the cluster can be estimated as 0.4 Myr (see § 4.2 for detail). H I and CO data are the same as that for Fig. 5.

In Figure 7 we note that Cloud 2-N is distributed along the tangential direction of the SNR shell, while Cloud 2-S extends slightly inward. A close investigation of the SNR H I shell in a velocity range similar to that of the CO clouds (-102 to -105 km s^{-1}) reveals that another shell-like structure is associated with Cloud 2-S (Fig. 8). This substructure in the H I map can also be seen in the H I velocity channel map at -104.5 km s^{-1} in Figure 1 in Stil & Irwin (2001). We denote it as Cavity 2B, since it encompasses Cavity 2 of Stil & Irwin. A closer look at the molecular cloud (Fig. 7) shows that the southern half of Cloud 2 appears to be perturbed by Cavity 2B at around R.A.$_{\rm J2000.0} = 02^{\rm h}48^{\rm m}30^{\rm s}$, decl.$_{\rm J2000.0} = 58°26′$.

We also found that both embedded clusters in Cloud 2 (the Cloud 2-S cluster and the IRS 3 minicluster) are located on the western side of the cloud cores (see Fig. 7, *red plus signs*). This appears to imply that the shock from the western side, presumably from Cavity 2B, caused star formation in Cloud 2-S. Therefore, we propose that *strong compressions* of Cloud 2-S from the combination of the SNR shell and Cavity 2B caused cluster-mode star formation, whereas isolated-mode star formation occurred in Cloud 2-N. This may be one of the best examples that clearly supports the theoretical and observational suggestions that high pressure is the trigger of cluster-mode star formation (e.g., Elmegreen 1998, 2004).

The center of Cavity 2B is at about $(l, b) = (137.59°, -1.16°)$, or R.A.$_{\rm J2000.0} = 02^{\rm h}46^{\rm m}53^{\rm s}$, decl.$_{\rm J2000.0} = +58°23′$, with a radius of about 12′ (about 45 pc). Cavity 2B could be either a smaller (thus, younger) adjacent SNR shell or a hole in the SNR shell like Cavity 1 and Cavity 2 in Stil & Irwin (2001). Although Cavity 1 appears to be a hole in the SNR shell rather than another SNR shell (Stil & Irwin 2001), we confirmed a sign of an expanding shell for Cavity 2B in an H I position-velocity map made with the Canadian Galactic Plane Survey (CGPS) data. Because we could not identify any radio continuum source inside Cavity 2B using the NRAO/VLA Sky Survey (NVSS) map (VLA 1.4 GHz), Cavity 2B does not seem to be powered by star-forming regions, and it could be another young SNR shell. Because this area around $(l, b) = (137.5°, -1.0°)$ on the SNR shell appears to be crowded with H I clouds throughout the velocity range of the expanding

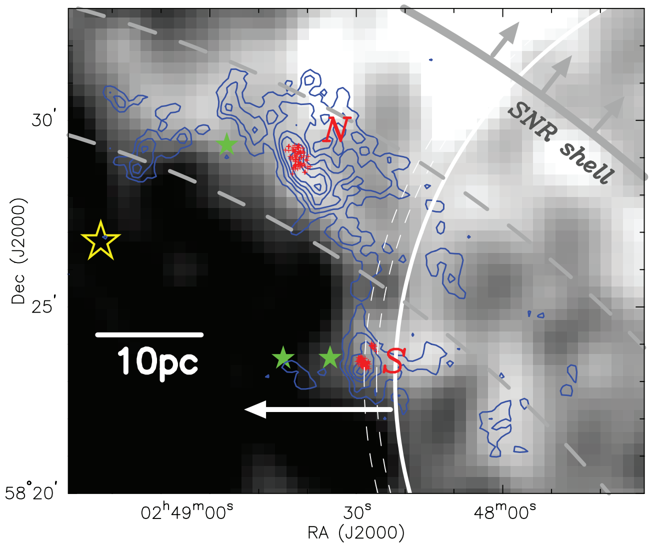

FIG. 7.—Relationship of the H I shells, Cloud 2 (*blue contours*), and the embedded clusters (*red plus signs*). The outer edge of the SNR shell, GHS 138-01-94, is shown by a solid gray curve, while the edge of Cavity 2B (see text) is shown by a solid white curve. Cloud 2-N is distributed between the two dashed gray curves, whereas Cloud 2-S appears to be pushed back inside the shell by the expansion of Cavity 2B. The cluster-mode star formation in Cloud 2-S occurs at the shock front facing Cavity 2B. The H I and CO images are the same as for Fig. 4. The open yellow star and filled green stars show the locations of the visible early-type star MR-1 and the bright NIR sources, respectively.

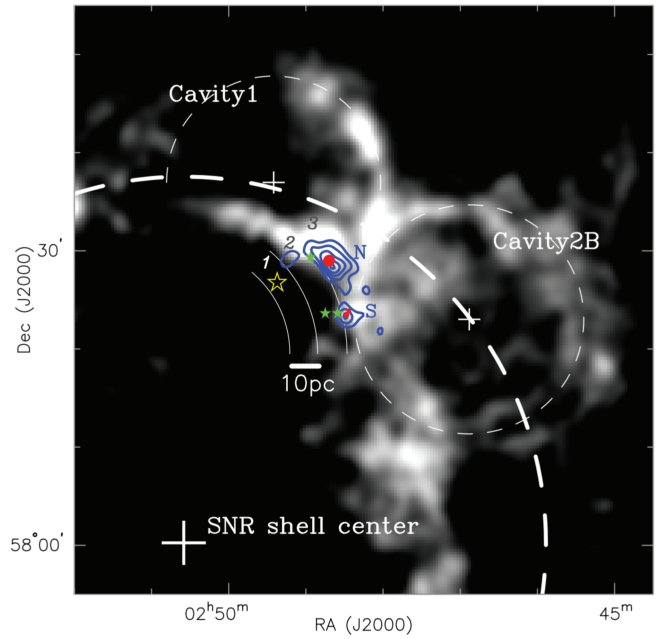

FIG. 8.—Cloud 2 and the associated members in the H I 21 cm gray-scale image. Cloud 2 is shown with ^{12}CO contours, and its members are shown with an open yellow star (visible early-type star MR-1), filled green stars (bright NIR sources), and red circles (two embedded clusters). Progressive star formation from the inner side of the shell toward the edge (from zone 1 to 2, then 3) is visible in this image. The CO data are the same as those for Figs. 1 and 4, except for the contour interval. The H I data from CGPS are integrated over a velocity range from −102 to −105 km s^{-1}, which shows the adjacent cavities clearly.

shell (see Fig. 1 in Stil & Irwin 2001), another interpretation is that Cavity 2B is just a group of in situ H I clouds that were distributed before the SN explosion. Cloud 2, powered by the main SNR shell (GSH 138-01-94), may have collided with the H I clouds, which caused the strong compression that stimulated the formation of the Cloud 2-S clusters.

4.4. *Summary of the SNR-triggered Star Formation History*

Figure 9 summarizes our interpretation of the star formation history in Cloud 2. The first-generation star (MR-1) and second-generation stars (the bright NIR sources) do not seem to accompany a cluster like that for the third-generation stars in the Cloud 2-N and 2-S clusters. This may suggest that those early-generation stars were born in an isolated mode without accompanying clusters. Although the ages of the clusters were estimated at ∼0.5 Myr (see discussion in § 4.2), it is hard to determine when those early-generation high- to intermediate-mass stars were born. In view of their possible locations inside the SNR sphere (the projected distance from the shell center to the stars is about 75% of the shell radius), their ages should not be more than 2 Myr in view of the age of the SNR shell (∼3 Myr; see § 4.2), even after considering the slowing down of the shell expansion. This probable age for the second-generation bright NIR sources is consistent with our interpretation that they are Herbig Ae/Be stars, whose typical ages are 0.1 to a few Myr (van den Ancker et al. 1997). The probable age of <2 Myr is also consistent with the first-generation star, MR-1, which is most likely in the main-sequence phase in view of its very short pre-main-sequence timescale (∼0.1 Myr; Bernasconi & Maeder 1996) for a large mass (∼20 $M_\odot$). Most of the red sources scattered in the field in Figure 1 are background galaxies, although some of them might be stars formed with the first- and second-generation high- to intermediate-mass stars. Note that the faint companions of the bright NIR stars, IRS 4 and 5, are distributed to the west. This might show the trace of progressive star formation: first, bright intermediate-mass stars were born, then the

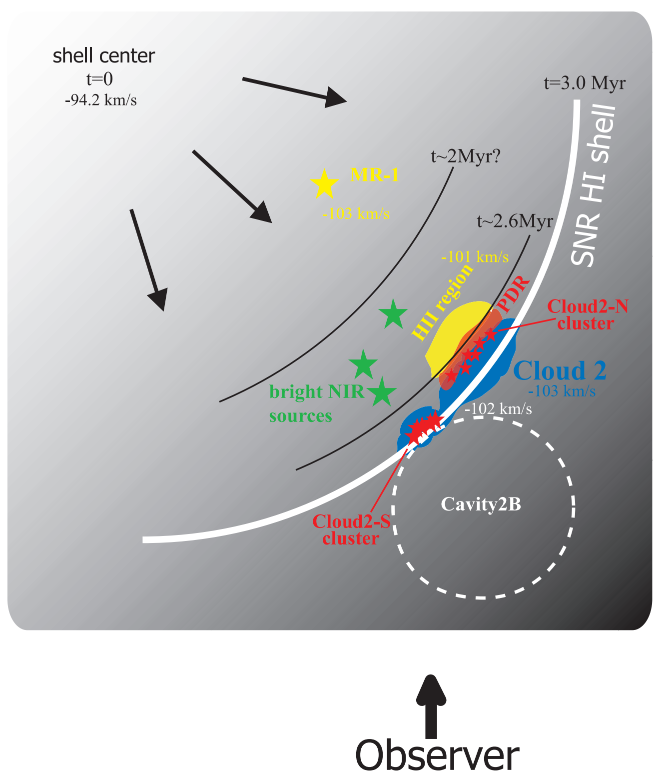

FIG. 9.—Schematic view of progressive star formation by the SNR shell. The scales and viewing angles are arbitrary. The times shown are counted from the time of the explosion of the SN. The radial velocities of the objects are shown (shell center, H I, and Cloud 2, Stil & Irwin 2001; H II, de Geus et al. 1993; MR-1, Russeil et al. 2007). See the text for detailed discussion.

low-mass stars just to the west formed from the remaining cloud. Future kinematical study of all those cloud members with NIR echelle spectroscopy may shed light on the dynamical processes that happened during triggered star formation.

5. LINK TO THE EARLY PHASE OF THE GALAXY'S FORMATION

Ferguson et al. (1998) have pointed out that the outskirts of spiral galaxies in the local universe have characteristics similar to those of high-redshift damped Lyα systems, as well as giant low surface brightness galaxies, in that they have low gas surface densities (yet high gas fractions compared to stars), low metallicities, and long dynamical timescales. The irregular (Im) dwarf galaxies, which are generally dominated in the optical by their younger stellar populations, also have similar characteristics (Hunter et al. 2006). They are usually lower in luminosity and surface brightness, more gas-rich with a lower metallicity and dust content, and form stars without the benefit of spiral density waves. All these characteristics suggest that the irregular dwarf galaxies are representative of the nature of star formation in the early universe (Hunter et al. 2006; Hunter & Elmegreen 2004, 2006). However, the distance to the nearest Im galaxy (LMC) is 50 kpc, while the distance to the EOG is 10–20 kpc. The proximity of the EOG enables us to resolve star cluster members with ground-based seeing resolution (see Yasui et al. 2006, 2008), and spectroscopic study is also possible with 8 m class telescopes even for low-mass stars (e.g., down to $K = 19-20$ mag). The gas content can also be studied in detail statistically (Snell et al. 2002) and with various molecular lines (Lubowich et al. 2004; Ruffle et al. 2005; Brand & Wouterloot 2007). Therefore, the EOG is an excellent place to study the star formation processes that were present during the early epoch of galaxy formation and that are still present in Im galaxies (Hunter et al. 2006).

The metallicity of outer galaxy disks, Im galaxies, low-metallicity blue compact dwarf galaxies (Kunth & Ostlin 2000), and damped Lyα systems is observed down to $[\mathrm{Fe/H}] \sim -3$ (e.g., Pettini 2004). This metallicity range traces the critical phases of early Galaxy formation, when the major components, such as the halo, thick disk, bulge, and thin disk, formed (e.g., Fig. 3 in Buser 2000; Freeman & Bland-Hawthorn 2002). The typical metallicity of the outer galaxy regions ($-1.5 < [\mathrm{Fe/H}] < -0.5$) suggests that they represent the late phase of halo formation and the early phase of thick-disk formation. Despite many extensive studies (e.g., Bensby et al. 2007 and references therein), the origin and role of the thick disk in our Galaxy are not well understood, even decades after its discovery (Gilmore & Reid 1983). Although the study of abundance patterns recorded in very low metallicity stars ($[\mathrm{Fe/H}] < -2.5$) provides a vital clue to the star formation process in the very early epoch of galaxy formation (Audouze & Silk 1995; Shigeyama & Tsujimoto 1998; Tsujimoto & Shigeyama 1998), this successful "archeological method" cannot be applied to the metallicity range of the thick disk, because the abundance patterns of the formed stars are significantly affected by the Galactic global chemical evolution of the interstellar medium, from which the stars are formed. The observational study of the outer Galaxy region may directly reveal the details of the star formation process during the formation of the thick disk, which took place at $z \sim 2$ ($\sim$10 Gyr ago), to shed light on the origin and role of this important Galactic component.

In the last decade, the formation of Population III stars (the "first stars") has been extensively studied theoretically (Abel et al. 2002; Bromm et al. 2002; Nakamura & Umemura 2001), not only for its own sake, but because of its direct relation to the reionization of the early universe and galaxy formation at an early epoch (see, e.g., Yoshida 2006). The recent advancement in the study of extremely metal-poor stars (Christlieb et al. 2002; Beers & Christlieb 2005), which are the potential relics of Population III stars, boosted the examination of early-phase galaxy formation through the study of abundance patterns recorded in very low metallicity stars at a very early epoch. Although theoretical studies suggest that the star formation physics in the metallicity range of the outer galaxy regions should not significantly differ from that of the solar metallicity (e.g., Omukai 2000), the observational study of the regions in this "niche" metallicity range establishes a good link between the very low and solar metallicity ranges, thereby revealing important astronomical processes in this metallicity range.

It is most likely that SN-triggered star formation was the major process by which stars formed in the early epoch of galaxy formation because of the lack of other major star formation triggers, such as density waves in spiral galaxies. Tsujimoto et al. (1999) first formulated SN-triggered star formation in the early epoch of Galaxy formation by utilizing the abundance pattern recorded in very low metallicity stars in our Galaxy (see also Tsujimoto et al. 2002). They successfully constrained the star formation efficiency and mass function during the formation of the Galactic halo. With clear SN-triggered star formation signatures, Cloud 2 and probably other EOG clouds are excellent places to confirm the predictions from near-field cosmology.

6. CONCLUSION

We present a detailed study of star formation in Cloud 2, which is one of the active star-forming regions in the EOG and one of the farthest star-forming regions, with a probable Galactic radius of $\sim$20 kpc. Cloud 2 has a quite different environment from that of the solar neighborhood, including lower metallicity, much lower gas density, and small or no perturbation from the spiral arms. As such, it is a useful analog for the star formation process in an early epoch of our Galaxy. In particular, the study of the EOG may shed light on the origin and role of the thick disk, whose metallicity range matches well with that of the EOG.

Our main results are as follows:

1. With new wide-field near-infrared (NIR) imaging that covers the entire Cloud 2, we discovered two young embedded star clusters located in the two dense cores of the cloud.
2. The two embedded clusters show a distinct morphology difference: the one in the northern molecular cloud core is a loose association with an isolated star formation mode, while the one in the southern molecular cloud core is a dense cluster with a cluster star formation mode.
3. Using our NIR and ^{12}CO data, as well as H I, radio continuum, and *IRAS* data from the archives, we show clear evidence of sequential star formation triggered by the large nearby SNR, GSH 138-01-94.
4. We propose that the high compression resulting from a combination of the SNR shell and an adjacent shell caused the dense cluster formation in the southern core.

We are grateful to the UH 2.2 m telescope staff, especially John Dvorak and Andrew Pickles, for their support during the QUIRC observations. We also thank Takuji Tsujimoto for fruitful discussions and suggestions about star formation in the early epoch of the Galaxy's formation. We thank the anonymous referee for careful reading and thoughtful suggestions that significantly improved this paper. This research was supported by a Grant-in-Aid for Encouragement of Scientists (A) of the Ministry of Education, Science, Culture, and Sports in Japan (No. 11740128). N. K. was partly supported by a Japan Society for the Promotion of Science postdoctoral fellowship for research abroad. N. K. is also very grateful to the staff of the Institute for Astronomy, University of Hawaii, for their warm support during his stay in Honolulu.

REFERENCES

Abel, T., Bryan, G. L., & Norman, M. L. 2002, Science, 295, 93
Allen, L., et al. 2007, in Protostars and Planets V, ed. B. Reipurth, D. Jewitt, & K. Keil (Tucson: Univ. Arizona Press), 361
Audouze, J., & Silk, J. 1995, ApJ, 451, L49
Beers, T. C., & Christlieb, N. 2005, ARA&A, 43, 531
Bensby, T., Zenn, A. R., Oey, M. S., & Feltzing, S. 2007, ApJ, 663, L13
Bernasconi, P. A., & Maeder, A. 1996, A&A, 307, 829
Brand, J., & Wouterloot, J. G. A. 1995, A&A, 303, 851
———. 2007, A&A, 464, 909
Brewer, M.-M., & Carney, B. W. 2006, AJ, 131, 431
Bromm, V., Coppi, P. S., & Larson, R. B. 2002, ApJ, 564, 23
Buser, R. 2000, Science, 287, 69
Christlieb, N., et al. 2002, Nature, 419, 904
Condon, J. J., Cotton, W. D., Greisen, E. W., Yin, Q. F., Perley, R. A., Taylor, G. B., & Broderick, J. J. 1998, AJ, 115, 1693
de Geus, E. J., Vogel, S. N., Digel, S. W., & Gruendl, R. A. 1993, ApJ, 413, L97
Digel, S., de Geus, E., & Thaddeus, P. 1994, ApJ, 422, 92
Drilling, J. S., & Landolt, A. U. 2000, in Allen's Astrophysical Quantities, ed. A. N. Cox (4th ed.; New York: AIP), 381
Dyson, J. E., & Williams, D. A. 1997, The Physics of the Interstellar Medium (2nd ed.; Bristol: IOP)
Elmegreen, B. G. 1998, in ASP Conf. Ser. 148, Origins, ed. C. E. Woodward, J. M. Schull, & H. A. Thronson Jr. (San Francisco: ASP), 150
———. 2002, ApJ, 577, 206
———. 2004, in ASP Conf. Ser. 322, The Formation and Evolution of Massive Young Star Clusters, ed. H. J. G. L. M. Lamers, L. J. Smith, & A. Nota (San Francisco: ASP), 277
Ferguson, A. M. N., Gallagher, J. S., & Wyse, R. F. G. 1998, AJ, 116, 673
Freeman, K., & Bland-Hawthorn, J. 2002, ARA&A, 40, 487
Gilmore, G., & Reid, N. 1983, MNRAS, 202, 1025
Heyer, M. H., Brunt, C., Snell, R. L., Howe, J. E., & Schloerb, F. P 1998, ApJS, 115, 241
Hunter, D. A., & Elmegreen, B. G. 2004, AJ, 128, 2170
———. 2006, ApJS, 162, 49
Hunter, D. A., Elmegreen, B. G., & Martin, E. 2006, AJ, 132, 801
Kobayashi, N., & Tokunaga, A. T. 2000, ApJ, 532, 423
———. 2001, in ASP Conf. Ser. 231, Tetons 4: Galactic Structure, Stars and the Interstellar Medium, ed. C. E. Woodward, M. D. Bicay, & J. M. Schull (San Francisco: ASP), 83
Kunth, D., & Ostlin, G. 2000, A&A Rev., 10, 1
Lada, C. J., & Lada, E. A. 2003, ARA&A, 41, 57
Lada, E. A., Strom, K. M., & Myers, P. C. 1993, in Protostars and Planets III, ed. E. H. Levy & J. I. Irving (Tucson: Univ. Arizona Press), 245
Lubowich, D. A., Brammer, G., Roberts, H., Millar, T. J., Henkel, C., & Pasachoff, J. M. 2004, in Origin and Evolution of the Elements, ed. A. McWilliam & M. Rauch (Pasadena: Carnegie Obs.), http://www.ociw.edu/ociw/symposia/series/symposium4/proceedings.html
McLachlan, A., & Nandy, K. 1985, MNRAS, 215, 473
Muzzio, J. C., & Rydgren, A. E. 1974, AJ, 79, 864
Nakamura, F., & Umemura, M. 2001, ApJ, 548, 19
Nakanishi, H., & Sofue, Y. 2003, PASJ, 55, 191
Omukai, K. 2000, ApJ, 534, 809
Pettini, M. 2004, in Cosmochemistry: The Melting Pot of the Elements, ed. C. Esteban et al. (Cambridge: Cambridge Univ. Press), 257
Rolleston, W. R. J., Smartt, S. J., Dufton, P. L., & Ryans, R. S. I. 2000, A&A, 363, 537
Ruffle, P. 2006, Ph.D. thesis, Univ. Manchester, chap. 13
Ruffle, P., Millar, T., Roberts, H., Henkel, C., & Lubowich, D. 2005, in IAU Symp. 231, Astrochemistry Throughout the Universe, ed. D. C. Lis, G. A. Blake, & E. Herbst (Cambridge: Cambridge Univ. Press), 1
Ruffle, P. M. E., Millar, T. J., Roberts, H., Lubowich, D. A., Henkel, C., Pasachoff, J. M., & Brammer, G. 2007, ApJ, 671, 1766
Russeil, D., Adami, C., & Georgelin, Y. M. 2007, A&A, 470, 161
Ryan, S. G., Norris, J. E., & Beers, T. C. 1996, ApJ, 471, 254
Santos, C. A., Yun, J. L., Clemens, D. P., & Agostinho, R. J. 2000, ApJ, 540, L87
Shigeyama, T., & Tsujimoto, T. 1998, ApJ, 507, L135
Smartt, S. J., Dufton, P. L., & Rolleston, W. R. J. 1996, A&A, 305, 164
Smartt, S. J., & Rolleston, W. R. J. 1997, ApJ, 481, L47
Snell, R. L., Carpenter, J. M., & Heyer, M. H. 2002, ApJ, 578, 229
Stil, J. M., & Irwin, J. A. 2001, ApJ, 563, 816
Testi, L., Palla, F., & Natta, A. 1999, A&A, 342, 515
Tielens, A. G. G. M. 2005, The Physics and Chemistry of the Interstellar Medium (Cambridge: Cambridge Univ. Press)
Tokunaga, A. T. 2000, in Allen's Astrophysical Quantities, ed. A. N. Cox (4th ed.; New York: AIP), 143
Tsujimoto, T., & Shigeyama, T. 1998, ApJ, 508, L151
Tsujimoto, T., Shigeyama, T., & Yoshii, Y. 1999, ApJ, 519, L63
———. 2002, ApJ, 565, 1011
van den Ancker, M. E., The, P. S., Tjin A Djie, H. R. E., Catala, C., de Winter, D., Blondel, P. F. C., & Waters, L. B. F. M. 1997, A&A, 324, L33
Westerhout, G., & Wendlandt, H.-U. 1982, A&AS, 49, 143
Wouterloot, J. G. A., & Brand, J. 1989, A&AS, 80, 149
Wouterloot, J. G. A., Brand, J., Burton, W. B., & Kwee, K. K. 1990, A&A, 230, 21
Yasui, C., Kobayashi, N., Tokunaga, A. T., Terada, H., & Saito, M. 2006, ApJ, 649, 753
———. 2008, ApJ, 675, 443
Yoshida, N. 2006, NewA Rev., 50, 19